Singularity Analysis of a Class of Composite Serial In-Parallel Robots

Nabil Simaan and Moshe Shoham, *Member, IEEE*

***Abstract*—This paper presents the singularity analysis of a family of 14 composite serial in-parallel six degree-of-freedom robots, having a common parallel submechanism. The singular configurations of this class of robots are obtained by applying line geometry methods to a single, augmented Jacobian matrix whose rows are Plücker coordinates of the lines governing the submechanism motion. It is shown that this family of robots possesses three general parallel singularities that are attributed to the general complex singularity. The results were verified experimentally on a prototype of a composite serial in-parallel robot that was synthesized and constructed for use in medical applications.**

***Index Terms*—Composite serial in-parallel robots, geometric approach, line geometry, parallel robots, RSPR robot, singularity analysis.**

I. Introduction

NUMEROUS researchers, e.g., [1]–[9], have investigated singularity conditions of parallel robots since complete knowledge of the singular regions within their workspace is essential for design and control purposes. Singularity analysis is based on the instantaneous kinematics of the manipulator, which is described by

$$\mathbf{A}\dot{\mathbf{x}} = \mathbf{B}\dot{\mathbf{q}} \tag{1}$$

where for n degrees-of-freedom (DOF) manipulator, $\mathbf{A}$ and $\mathbf{B}$ are an $n \times 6$ and an $n \times n$ matrices referred to in this paper as the instantaneous direct and inverse kinematics (IDK, IIK) matrices, respectively. These matrices were used by Gosselin and Angeles [2] for singularity analysis and were respectively called the direct kinematics and inverse kinematics matrices in [10], or direct kinematics and inverse kinematics Jacobians in [11]. $\dot{\mathbf{x}}$ is the moving platform twist, and $\dot{\mathbf{q}}$ is the active joints' speeds. For fully parallel robots, the IIK matrix, $\mathbf{B}$, is a diagonal one [4]. Hence, the common definition for the Jacobian matrix of parallel robots takes the form $\mathbf{J} = \mathbf{B}^{-1}\mathbf{A}$ and the IIK problem is defined by $\dot{\mathbf{q}} = \mathbf{J}\dot{\mathbf{x}}$.

Based on rank-deficiency of the matrices $\mathbf{A}$ and $\mathbf{B}$, Gosselin and Angeles [2] divided the singular configurations into three cases: the first, when only $\mathbf{A}$ is singular; the second when only $\mathbf{B}$ is singular; and the third when both $\mathbf{A}$ and $\mathbf{B}$ are singular. In this paper, we adopt the terminology in [10] and refer to the singular configurations associated with singularities of the instantaneous direct kinematics matrix $\mathbf{A}$ and the instantaneous inverse kinematics matrix $\mathbf{B}$ as *parallel* and *serial singularities*, respectively.

Hunt *et al.* [3] discussed the singular configurations in serial, parallel, and composite serial and in-parallel robots, by using motion and action screws. They showed that a work-piece grasped by a serial kinematic chain robot can only lose DOF (or gain constraint) and a work-piece grasped by fully in-parallel manipulator can only gain DOF (or lose constraint). A composite serial in-parallel manipulator can either lose or gain DOF.

In a singular configuration, the relation between the input variables' velocities (active joints' speeds) and the output variables' velocities (linear/angular velocities of the end effector) is not fully defined. For serial robots with six DOF, a configuration is singular when the instantaneous input–output map $\dot{\mathbf{x}} = \mathbf{J}\dot{\mathbf{q}}$ is singular. For parallel robots with $n < 6$, there exists a 6×6 matrix $\mathbf{A}_{\mathrm{s}}$ that governs the static equilibrium of the moving platform. This matrix relates the internal forces/moments, $\boldsymbol{\tau}_{\mathbf{in}}$, acting on the moving platform with the wrench $\mathbf{s}_{\mathrm{e}}$ applied by the moving platform on its environment

$$\mathbf{A}_{\mathrm{s}}\boldsymbol{\tau}_{\mathbf{in}} = \mathbf{s}_{\mathrm{e}}. \tag{2}$$

The internal forces $\boldsymbol{\tau}_{\mathbf{in}}$ acting on the moving platform are divided into two groups. The first group represents the active joints' intensities $\{\tau_1 \ldots \tau_n\}$. The second group $\{\tau_{n+1} \ldots \tau_6\}$ represents the intensities of the passive forces. These passive forces stem from the kinematic constraints imposed by the joint dyads of the links connected to the moving platform. The first n columns of $\mathbf{A}_{\mathrm{s}}$ are the action screws associated with the active joints. The remaining $6 - n$ columns are the action screws associated with the constraints of the passive joints.

Singularity of uncertainty configuration occurs when the column space of $\mathbf{A}_{\mathrm{s}}$ has a dimension less than six. If $\mathbf{A}_{\mathrm{s}}$ has a rank of $m < 6$, then the manipulator cannot resist external wrenches that belong to a $(6 - m)$-dimensional space and the manipulator is in uncertainty configuration [3], [8].

The derivation of the Jacobian matrix from $\mathbf{A}_{\mathrm{s}}$ is immediate by writing the expression for the work rate of the forces/moments acting on the moving platform. The work done by the constraints is zero. This leads to the result that the first n columns of $\mathbf{A}_{\mathrm{s}}$ are the rows of the $n \times 6$ Jacobian matrix. This result emphasizes the importance of the matrix $\mathbf{A}_{\mathrm{s}}$ for complete singularity analysis. For robots with $n < 6$, the Jacobian matrix by itself is not sufficient to determine all conditions for singularity.

Since the IDK matrix is composed of line coordinates, the analysis of parallel singularities is reduced to determining the geometric conditions for linear dependence between these lines, [1], [13].

Dandurand [14] addressed the problem of rigidity conditions of compound spatial grids by using line geometry. Since the Ja-

Manuscript received June 12, 2000; revised January 9, 2001. This paper was recommended for publication by Associate Editor F. Park and Editor I. Walker upon evaluation of the reviewers' comments.

The authors are with the Robotics Laboratory, Department of Mechanical Engineering, Technion–Israel Institute of Technology, Haifa 32000, Israel (email: nabil@tx.technion.ac.il; shoham@tx.technion.ac.il).

Publisher Item Identifier S 1042-296X(01)06737-4.

1042-296X/01$10.00 © 2001 IEEE

TABLE I
A FAMILY OF 14 COMPOSITE SERIAL IN-PARALLEL ROBOTS

RSPR	PSPR	HSPR	PPSR	RRSR
HHSR	RPSR	HRSR	HPSR	RHSR
PRSR	PHSR	USR	CSR	

cobian matrix of fully-parallel Stewart–Gough robots consists of Plücker line coordinates of the lines along the prismatic actuators, [2], the singularity analysis of these robots is based on finding geometrical conditions for linear dependence between these lines. Following Dandurand's observations, a group of researchers, [1], [7], [15], [16] investigated the parallel singularities of parallel robots using line geometry. Notash [8] used line geometry to investigate redundant three-branch platform robots and their preferable actuation distribution in order to eliminate singularities. Hao and McCarthy [13] discussed the conditions of joint arrangements that ensure line-based singularities in platform robots. They showed that in order to have line-based singularities, the kinematic chains should not transmit torque to the moving platform. Even though the family of robots investigated in the present work does not fulfill this condition, nevertheless a special Jacobian formulation allows maintaining the line-based expression of the Jacobian matrix of the common parallel submechanism (defined in Section III) of this class of robots.

Unlike fully parallel robots that have a diagonal nonsingular IIK matrix, $\mathbf{B}$ (for a nonzero length of the linear actuators), composite serial in-parallel robots require both matrices $\mathbf{A}$ and $\mathbf{B}$ to be examined for singularity. Singularity of matrix $\mathbf{B}$ indicates a loss of DOF and singularity of matrix $\mathbf{A}$ indicates gain in DOF [2].

The structure of a family of composite serial in-parallel robots is presented next (Sections II and III) and its parallel singularities are derived based on line geometry (Sections V and VI).

II. A FAMILY OF COMPOSITE SERIAL IN-PARALLEL ROBOTS

A class of 14 composite serial in-parallel robots is listed in Table I. Each robot is represented by a code depicting the structure of its kinematic chains from the base platform to the moving platform. The letter R stands for a revolute joint, S for spherical, P for prismatic, U for universal (Hooke's), C for cylindrical, and H for helical joint.

All the robots of this family have three similar kinematic chains connected to a moving platform by revolute joints. The last links in the kinematic chains, $A_i,\ i = 1 \ldots 3$, are passive binary spherical-revolute (S-R) dyads. Table I depicts all the 14 possible combinations of joints constituting connectivity that equals six between the base and the moving platform. Although some investigations use special distribution of actuators [17] and passive sliders [18]–[20] to simplify the direct kinematics solution or to minimize singularities via redundancy [8], we limit our discussion to symmetrical nonredundant robots with three identical kinematic chains and symmetrical distribution of actuators.

III. LINE-BASED FORMULATION OF THE JACOBIAN

The formulation of the Jacobian matrix based on static analysis is described next. The same formulation can also be achieved by writing loop-closure equations and taking their derivative with respect to time.

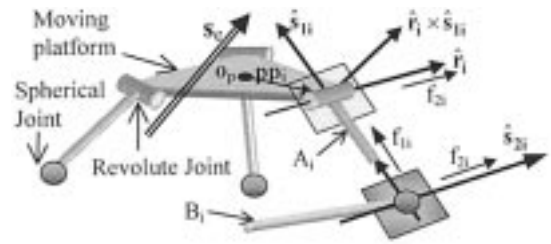

Fig. 1. Force transmission in the tripod mechanism.

All the robots in Table I have the same system of constraint wrenches acting on the moving platform. This stems from the fact that all these robots have a common tripod mechanism composed of a moving platform and three passive S-R joint dyads (Fig. 1).

Nomenclature

i	Index referring to i'th kinematic chain, $i = 1, 2, 3$.
A_i	i'th link of the tripod mechanism.
$\mathbf{o}_\mathrm{p}$	Moving platform's center point.
$\hat{\mathbf{r}}_i$	Unit vector along the i'th revolute joint.
$\hat{\mathbf{s}}_{1i}$	Unit vector along link A_i (Fig. 1).
$\hat{\mathbf{s}}_{2i}$	Unit vector parallel to $\hat{\mathbf{r}}_i$ and passing through the i'th spherical joint center.
f_{2i}	Magnitude of force acting on A_i, along $\hat{\mathbf{s}}_{2i}$.
$\mathbf{f}_1, \mathbf{f}_2$	Force vectors along links A_i and along $\hat{\mathbf{s}}_{2i}$, respectively.
$\mathbf{s}_\mathrm{e}$	Six-dimensional external wrench applied by the moving platform on its environment. $\mathbf{s}_\mathrm{e} = [\mathbf{f}_\mathrm{e}, \mathbf{t}_\mathrm{e}]$, where $\mathbf{f}_\mathrm{e}$ and $\mathbf{t}_\mathrm{e}$ are the resultant external force/moment, respectively.
${}^w\mathbf{R}_\mathrm{p}$	Rotation matrix from platform-attached coordinate system, P, to world coordinate system, W.
$\mathbf{pp}_i$	A vector from $\mathbf{o}_\mathrm{p}$ to a point on $\hat{\mathbf{r}}_i$ (written in platform-attached coordinate system).

Link A_i is connected to the moving platform by a passive revolute joint and to link B_i by a passive spherical joint. Consequently, it is capable of exerting on the platform a static force in a direction spanned by the flat pencil of $\hat{\mathbf{s}}_{1i}$ and $\hat{\mathbf{r}}_i$, and a moment in the direction of $\hat{\mathbf{r}}_i \times \hat{\mathbf{s}}_{1i}$ (Fig. 1). Link B_i can exert on link A_i, through the center of the spherical joint, a static force in a direction defined by the flat pencil of $\hat{\mathbf{s}}_{1i}$ and $\hat{\mathbf{s}}_{2i}$. Therefore, we decompose the force transmitted from link B_i to A_i into two components—one of magnitude f_{1i} and in the direction of $\hat{\mathbf{s}}_{1i}$ and the second of magnitude f_{2i} and in the direction of $\hat{\mathbf{s}}_{2i}$.

Equations (3) and (4) result from static equilibrium of forces and moments about the center point $\mathbf{o}_\mathrm{p}$

$$\sum_{i=1}^{3} f_{1i}\hat{\mathbf{s}}_{1i} + \sum_{i=1}^{3} f_{2i}\hat{\mathbf{s}}_{2i} - f_\mathrm{e} = \mathbf{0} \tag{3}$$

$$\sum_{i=1}^{3} {}^w\mathbf{R}_\mathrm{P}\mathbf{pp}_i \times f_{1i}\hat{\mathbf{s}}_{1i} + \sum_{i=1}^{3} {}^w\mathbf{R}_\mathrm{p}\mathbf{pp}_i \times f_{2i}\hat{\mathbf{s}}_{2i} + \sum_{i=1}^{3} -\mathbf{s}_{1i} \times f_{2i}\hat{\mathbf{s}}_{2i} - \mathbf{t}_\mathrm{e} = \mathbf{0}. \tag{4}$$

Rewriting (3) and (4) in a matrix form yields

$$\begin{bmatrix} \hat{\mathbf{s}}_{1i} & \hat{\mathbf{s}}_{2i} \\ {}^{w}\mathbf{R}_{\mathrm{p}}\mathbf{p}\mathbf{p}_i \times \hat{\mathbf{s}}_{1i} & ({}^{w}\mathbf{R}_{\mathrm{p}}\mathbf{p}\mathbf{p}_i - \mathbf{s}_{1i}) \times \hat{\mathbf{s}}_{2i} \end{bmatrix} \begin{bmatrix} \mathbf{f}_1 \\ \mathbf{f}_2 \end{bmatrix} = \begin{bmatrix} \mathbf{f}_{\mathrm{e}} \\ \mathbf{t}_{\mathrm{e}} \end{bmatrix}. \tag{5}$$

For parallel robots, the expression connecting the associated active joints' intensities $\boldsymbol{\tau}$ with $\mathbf{s}_{\mathrm{e}}$ is given by $\boldsymbol{\tau} = \mathbf{J}^{-\mathrm{T}}\mathbf{s}_{\mathrm{e}}$. Equating this expression with (5) yields the Jacobian of the tripod mechanism $\tilde{\mathbf{J}}$.

$$\tilde{\mathbf{J}} = \begin{bmatrix} \hat{\mathbf{s}}_{1i} & \hat{\mathbf{s}}_{2i} \\ {}^{w}\mathbf{R}_{\mathrm{p}}\mathbf{p}\mathbf{p}_i \times \hat{\mathbf{s}}_{1i} & ({}^{w}\mathbf{R}_{\mathrm{p}}\mathbf{p}\mathbf{p}_i - \mathbf{s}_{1i}) \times \hat{\mathbf{s}}_{2i} \end{bmatrix}^{\mathrm{T}}. \tag{6}$$

The forces at the spherical joints are given by

$$\begin{bmatrix} \mathbf{f}_1 \\ \mathbf{f}_2 \end{bmatrix} = \tilde{\mathbf{J}}^{-\mathrm{T}} \begin{bmatrix} \mathbf{f}_{\mathrm{e}} \\ \mathbf{t}_{\mathrm{e}} \end{bmatrix}. \tag{7}$$

The rows of the Jacobian matrix of the tripod $\tilde{\mathbf{J}}$ are the Plücker line coordinates of the lines along the links $\hat{\mathbf{s}}_{1i}$ and the lines $\hat{\mathbf{s}}_{2i}$ (Fig. 1). These vectors can be found by the inverse kinematics of the tripod. Actually, the exact values of $\hat{\mathbf{s}}_{1i}$ and $\hat{\mathbf{s}}_{2i}$ are not needed since, as will be seen in Section VI, the singularity analysis is purely based on line geometry. In this analysis, the aim is to find the types of parallel singularities rather than the actual joint values in these singular configurations.

The group of robots in Table I shares the same tripod mechanism. The complete Jacobian matrix of this group is easily obtained by taking into account the force equilibrium at the spherical joints. By treating the remainder of the kinematic chains as serial chains, it is possible to obtain a relation between the forces f_{1i} and f_{2i} and the active joints' forces. The relation between the actuators' force intensities and the forces at the spherical joints is given by

$$\boldsymbol{\tau} = \mathbf{J}_{\mathrm{s}}^{\mathrm{T}} \begin{bmatrix} \mathbf{f}_1 \\ \mathbf{f}_2 \end{bmatrix} \tag{8}$$

where $\mathbf{J}_{\mathrm{s}}$ denotes the Jacobian matrix of the serial chains.

Substituting the expression for the forces at the spherical joints, one obtains

$$\boldsymbol{\tau} = \mathbf{J}_{\mathrm{s}}^{\mathrm{T}} \begin{bmatrix} \mathbf{f}_1 \\ \mathbf{f}_2 \end{bmatrix} = \mathbf{J}_{\mathrm{s}}^{\mathrm{T}} \tilde{\mathbf{J}}^{-\mathrm{T}} \mathbf{s}_{\mathrm{e}} \tag{9}$$

hence, the Jacobian of the complete manipulator is

$$\mathbf{J} = \mathbf{J}_{\mathrm{s}}^{-1} \tilde{\mathbf{J}}. \tag{10}$$

Comparing (10) with $\mathbf{J} = \mathbf{B}^{-1}\mathbf{A}$ (where $\mathbf{B}$ and $\mathbf{A}$ are the IIK and IDK matrices, respectively) shows that the IDK matrix, $\mathbf{A}$, and the IIK matrix, $\mathbf{B}$, are the Jacobian matrix of the tripod $\tilde{\mathbf{J}}$ and the Jacobian matrix of the serial chains $\mathbf{J}_{\mathrm{s}}$, respectively. Every manipulator of this class of manipulators has the same $\tilde{\mathbf{J}}$ matrix, but a different $\mathbf{J}_{\mathrm{s}}$ matrix. For example, the Jacobian matrices of the RSPR and the USR robots (Table I) were formulated in [24] using this method.

Based on the observation that $\tilde{\mathbf{J}}$ (the IDK matrix) is associated with the tripod mechanism, we will refer to it as the parallel submechanism since it leads to *parallel singularities* characterized by the addition of DOF to the moving platform (loss of constraint).

The formulation of $\tilde{\mathbf{J}}$ presents a matrix composed of lines of the parallel submechanism rather than screws of the whole robot as is derived, for example, in [21]. The result obtained in [22] presents a formulation of the Jacobian matrix of the PPSR (Table I) manipulator in [23] based on the use of reciprocal screws. The results of the derivation presented here accede with those of [22], but due to formulation of the matrix $\tilde{\mathbf{J}}$ it is possible to apply line geometry to analyze the parallel singularities.

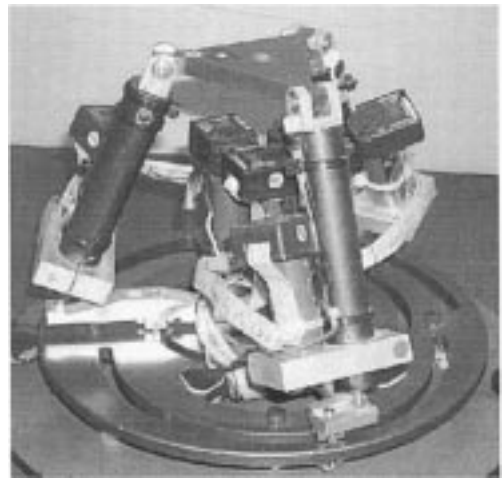

Fig. 2. RSPR robot.

IV. The RSPR Robot

The **RSP**R robot and another robot of this family, the **U**SR robot, were suggested by the authors as possible solutions for a medical robotic assistant for laparoscopic and knee surgery [24]–[28] (bold letters indicate the active joints). These robots were compared in terms of their workspace, dimensions, and required actuator forces, and the RSPR manipulator was chosen and constructed [41]. The prototype of the RSPR manipulator is shown in Fig. 2.

This manipulator consists of three identical kinematic chains connecting the base and the moving platform. Each chain contains a lower link rotating around a pivot perpendicular to the base platform and offset-placed from the center of the base. At the other end of the lower link, a prismatic actuator is attached by a spherical joint. The upper end of the prismatic actuator is connected to the moving platform by a revolute joint. The axes of the revolute joints constitute an equilateral triangle in the plane of the moving platform (Fig. 2).

This robot is distinguished by the location of the lower links revolute axes being placed offset from the center of the base platform as compared to the RRPS robot in [29].

V. Singularity Analysis Methodology

Based on the Jacobian matrix formulation of Section III, the singularity analysis for every robot in Table I is divided into two phases. The first phase deals with parallel singularities stemming from rank deficiency of the IDK matrix, $\mathbf{A}$ (referred to as $\tilde{\mathbf{J}}$ in Section III). The second phase deals with serial singularities of the IIK matrix, $\mathbf{B}$. In this paper, we present only the analysis of the parallel singularities, which is common to the 14 robots of Table I. In [27], the serial singularities of the RSPR and the USR robots were derived based on the determinants of their IIK matrices [24].

Since the IDK matrix $\tilde{\mathbf{J}}$ of a typical manipulator of this class is composed of the Plücker line coordinates of the parallel submechanism, we analyze its singularities using line geometry

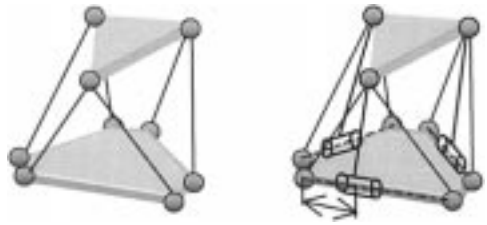

Fig. 3. Inverted tripod with variable moving platform laterals as an equivalent linkage to the TSSM [35].

technique. Readers interested in a background on line geometry should refer to [30]–[33], [12], and [34], where the last two books present the subject with its relevance to kinematics of mechanisms.

An inversion of the tripod of Fig. 1 was used in [35] and [36] as an equivalent mechanism of the Stewart–Gough 3-3 and 3-6 robots for solution of the direct kinematics and singularities [36] (Fig. 3). This suggests that the parallel singularities of the tripod mechanism are categorically the same as the Stewart–Gough 3-6 and 3-3 robots since, in both cases, the basic problem from line-geometry point of view is finding the possible linear dependencies between the lines of three *architectural flat pencils* (defined in next section) maneuvering in space. However, the equivalence is not direct since in Fig. 3 the equivalent mechanism of the triangular symmetric simplified manipulator (TSSM) [35] is an inversion of the tripod of Fig. 1 with variable laterals of its triangular platform. Thus, direct geometric interpretation of the singularities of the tripod of Fig. 1 is not possible by constructing its equivalent TSSM and analyzing it for singularity. The analysis given here shows how, by using geometric assumptions stemming from the architecture, one finds the direct geometric interpretation of the singularities with application to the working space of the moving platform. Indeed, our results accede with [1], [36], and [37], but we show that the interpretations of Fichter's [38] and Hunt's [39] singularities are different in our case, which has a direct impact on the motion capabilities of the moving platform.

Next, the analysis of parallel singularities begins from the general complex and works out all the cases up to flat pencil singularities. This way we economize the analysis since we ignore the special cases as, for example, flat pencil singularities that are special cases of bundle singularities.

VI. Singularity Analysis of the Parallel Submechanism

Fig. 4 presents a geometric interpretation of the Jacobian matrix $\tilde{\mathbf{J}}$ of the parallel submechanism (tripod) of the class of robots shown in Table I. We will use the symbols $\mathbf{l}_k,\ k = 1\ldots 6$, to refer to row number k in the tripod's Jacobian matrix $\tilde{\mathbf{J}}$, which are also the Plücker coordinates of lines $\mathbf{l}_1$, $\mathbf{l}_2$, $\mathbf{l}_3$, $\mathbf{l}_4$, $\mathbf{l}_5$, and $\mathbf{l}_6$ of Fig. 4. We employ line geometry to find all the configurations in which the rows of $\tilde{\mathbf{J}}$, i.e., lines $\mathbf{l}_1$, $\mathbf{l}_2$, $\mathbf{l}_3$, $\mathbf{l}_4$, $\mathbf{l}_5$, and $\mathbf{l}_6$ are linearly dependent.

First the relevant nomenclature for this section and a list of useful geometric relations, upon which all the following geometrical proofs are based, is presented.

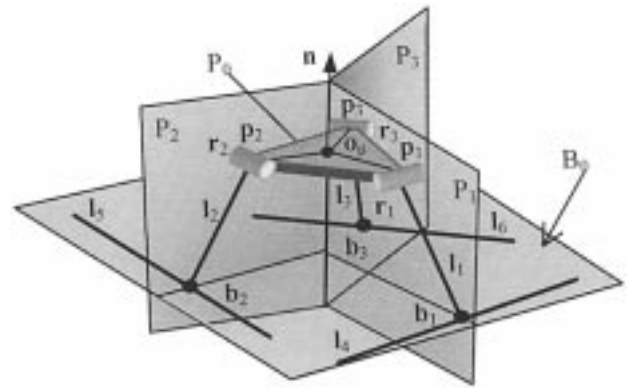

Fig. 4. Geometry of $\tilde{\mathbf{J}}$ and its associated lines $\mathbf{l}_1 \ldots \mathbf{l}_6$.

Nomenclature

The following symbols facilitate the formulation of the geometrical proofs in this section. All the symbols are explained herein and shown in Fig. 4.

$\mathbf{p}_i$	Center points of the revolute joints on the moving platform. $i = 1, 2, 3$.
$\mathbf{r}_i$	Vectors of the revolute joints' axes through $\mathbf{p}_i$.
$\mathbf{b}_i$	Center points of the spherical joints, $i = 1, 2, 3$.
$\mathbf{n}$	Normal to the moving platform plane through $\mathbf{o}_\mathrm{p}$.
$\mathrm{P}i$	Plane defined by $\mathbf{n}$ and point $\mathbf{p}_i$, $i = 1, 2, 3$.
$\mathrm{P0}$	Plane defined by points $\mathbf{p}_i$, $i = 1, 2, 3$.
$\mathrm{B0}$	Plane defined by points $\mathbf{b}_i$, $i = 1, 2, 3$. This plane is hereafter referred to as the tripod base plane.
jk	Flat pencil generated by lines $\mathbf{l}_j$ and $\mathbf{l}_k$. $k, j \in \{1, 2, 3, 4, 5, 6\}$, $k \neq j$.
X_{jk}	Flat pencil generated by lines $\mathbf{l}_j$ and $\mathbf{l}_k$ that belongs to category of flat pencils X. $(X_{jk} = X_{kj})$.
${}^{\mathrm{P}}X_{jk}$, ${}^{\mathrm{C}}X_{jk}$	Plane and center point of flat pencil X_{jk}.
$\mathbf{p}_j\mathbf{p}_k$	Line defined by points $\mathbf{p}_j$ and $\mathbf{p}_k$.
Γ	Group of the lines of $\tilde{\mathbf{J}}$, $\Gamma = \{\mathbf{l}_1, \mathbf{l}_2, \mathbf{l}_3, \mathbf{l}_4, \mathbf{l}_5, \mathbf{l}_6\}$.
C_{jk}	Group of lines of $\tilde{\mathbf{J}}$ excluding lines $\mathbf{l}_j$ and $\mathbf{l}_k$, $\mathrm{C}_{jk} = \{\mathbf{l}_n\colon\ \mathbf{l}_n \in \Gamma,\ n \neq j,\ n \neq k\}$

Lines and planes are regarded as sets of points. Therefore, the symbols $\cap$ and $\in$ have the same interpretation as for groups of points. Accordingly, the expression $\mathbf{a} \cap \mathbf{b}$ indicates the intersection of two lines, $\mathbf{a}$ and $\mathbf{b}$, in a common point, or the intersection of two planes, $\mathbf{a}$ and $\mathbf{b}$, along a common intersection line, or a line $\mathbf{a}$ piercing a plane $\mathbf{b}$. The expression $\mathbf{a} \in \mathbf{b}$ indicates that a point, $\mathbf{a}$, is on the line/plane, $\mathbf{b}$; or that a line, $\mathbf{a}$, lies in the plane $\mathbf{b}$.

Geometric Relations: The tripod mechanism of Fig. 4 features the following architectural geometric relations:

A1: Points $\mathbf{p}_i$ are not collinear.

A2: $\mathbf{b}_1 \in \mathrm{P1},\ \mathbf{b}_2 \in \mathrm{P2},\ \mathbf{b}_3 \in \mathrm{P3}$.

A3: $\mathbf{r}_1 \in \mathrm{P0},\ \mathbf{r}_2 \in \mathrm{P0},\ \mathbf{r}_3 \in \mathrm{P0}$.

A4: $\mathbf{l}_4 \parallel \mathbf{r}_1,\ \mathbf{l}_5 \parallel \mathbf{r}_2,\ \mathbf{l}_6 \parallel \mathbf{r}_3$.

A5: $\mathbf{r}_1 \perp \mathrm{P1},\ \mathbf{r}_2 \perp \mathrm{P2},\ \mathbf{r}_3 \perp \mathrm{P3}$.

A6: $\mathbf{p}_i \notin \mathbf{r}_j,\ i, j = 1, 2, 3,\ i \neq j$.

Corollaries: The following corollaries, Cr1 ... Cr3, result from geometric relations A1 ... A5. Each corollary is followed

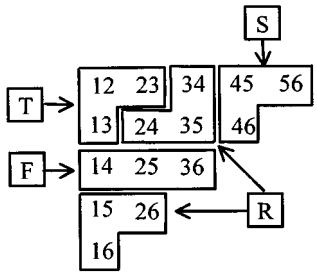

Fig. 5. Flat pencil groups.

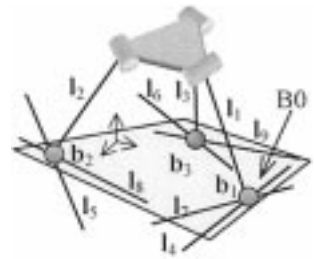

Fig. 6. The lines of Γ and lines $\mathbf{l}_7$, $\mathbf{l}_8$, and $\mathbf{l}_9$.

by brackets enclosing a list of geometric relations used to prove it.

Cr1 [A2]: $\mathbf{l}_1 \in \mathrm{P1},\ \mathbf{l}_2 \in \mathrm{P2},\ \mathbf{l}_3 \in \mathrm{P}_3$.

Cr2 [A3, A4]: $\mathbf{l}_4 \parallel \mathrm{P0},\ \mathbf{l}_5 \parallel \mathrm{P0},\ \mathbf{l}_6 \parallel \mathrm{P0}$.

Cr3 [A4, A5]: $\mathbf{l}_4 \perp \mathrm{P1},\ \mathbf{l}_5 \perp \mathrm{P2},\ \mathbf{l}_6 \perp \mathrm{P3}$.

Cr4 [A2, A4, A5]: $\mathbf{l}_4 \perp \mathbf{l}_1,\ \mathbf{l}_5 \perp \mathbf{l}_2,\ \mathbf{l}_6 \perp \mathbf{l}_3$.

Categories of Flat Pencils: We use flat pencils as a basic tool in deriving the singular configurations of the structure. It is therefore useful to enumerate all possible flat pencils.

A group of n lines in space can form up to $n(n-1)/2$ flat pencils. In our case, where $n = 6$, all possible 15 flat pencils of the tripod are grouped into four groups T, R, S, and F (Fig. 5), where each two-digit number jk represents a flat pencil formed by lines $\mathbf{l}_j$ and $\mathbf{l}_k$. Due to the similarity of the kinematic chains of the tripod, it is sufficient to analyze the singularity of only one member in each group.

We distinguish between *architectural flat pencils* and *temporary flat pencils* with temporary flat pencils being configuration-dependent, i.e., forming under certain conditions on the configuration variables and architectural flat pencil being configuration independent. Note that only category F includes architectural flat pencils.

Next, we adopt the code of Dandurand [14] to indicate the different line varieties. For each rank $-r\,(r < 6)$ line variety, we test all the cases in which more than r lines belong to this line group. This is tantamount to finding all the cases in which $r \leq \mathrm{rank}(\tilde{\mathbf{J}}) < 6$. For example, the term "bundle singularities," includes all the cases in which more than three lines, out of the six lines of Γ, belong to one bundle. This includes singularities with rank $3 \leq r < 6$.

A. Linear Complex Singularities

A group of six lines degenerates from the space variety to the linear complex variety in two ways. If all the six lines of the group belong to a general spatial linear pentagon, then singularity of the general complex occurs [30]. If all the six lines intersect one common line, then a singularity of the special complex occurs.

1) Six Lines in a General Complex (5A): Define lines $\mathbf{l}_7$, $\mathbf{l}_8$, and $\mathbf{l}_9$ as the intersection lines of the flat pencils F_{14}, F_{25}, F_{36} with the base plane B0, respectively (Fig. 6).

$$\mathbf{l}_7 = {}^{\mathrm{P}}\mathrm{F}_{14} \cap \mathrm{B0} \qquad \mathbf{l}_8 = {}^{\mathrm{P}}\mathrm{F}_{25} \cap \mathrm{B0} \qquad \mathbf{l}_9 = {}^{\mathrm{P}}\mathrm{F}_{36} \cap \mathrm{B0}.$$

Next, we prove that all six lines of $\Gamma = \{\mathbf{l}_1 \ldots \mathbf{l}_6\}$ belong to one general complex G if and only if lines $\mathbf{l}_7$, $\mathbf{l}_8$, and $\mathbf{l}_9$ intersect in one point (copunctal). The proof is based on the following theorem [32]. *A general linear complex has a pencil of lines in every plane and a pencil of lines through every point in space.*

This theorem means that, for a given general complex, every plane in space is associated with a flat pencil that belongs to it. Accordingly, the tripod base plane, B0, is associated with a flat pencil of lines of the general complex. Any line in B0 that does not belong to this flat pencil does not belong to the general complex and vise versa; any line belonging to this flat pencil belongs to the general complex.

There are six line quintuplets in $\Gamma = \{\mathbf{l}_1 \ldots \mathbf{l}_6\}$. Each one includes two architectural flat pencils. We consider the general complex G of lines generated by the two architectural flat pencils F_{14} and F_{25} and either line $\mathbf{l}_3$ or line $\mathbf{l}_6$ as a representative case to all other cases.

The following proof shows that all the six lines of $\Gamma = \{\mathbf{l}_1 \ldots \mathbf{l}_6\}$ belong to one general complex G, if and only if lines $\mathbf{l}_7$, $\mathbf{l}_8$, and $\mathbf{l}_9$ intersect in one point (copunctal).

Proof:

1) Lines $\mathbf{l}_7$, $\mathbf{l}_8$, and $\mathbf{l}_9$ fulfill $\mathbf{l}_7 \in \mathrm{F}_{14}$, $\mathbf{l}_8 \in \mathrm{F}_{25}$, $\mathbf{l}_9 \in \mathrm{F}_{36}$.
2) $\mathbf{l}_4$, $\mathbf{l}_5$, and $\mathbf{l}_6$ linearly depend on the flat pencils generated by the line pairs $(\mathbf{l}_1\ \mathbf{l}_7)$, $(\mathbf{l}_2\ \mathbf{l}_8)$, $(\mathbf{l}_3\ \mathbf{l}_9)$.
3) Lines $\mathbf{l}_7$ and $\mathbf{l}_8$ fulfill $\mathbf{l}_7 \in G$, $\mathbf{l}_8 \in G$ and $\mathbf{l}_7 \in B0$, $\mathbf{l}_8 \in B0$.
4) $\mathbf{l}_7$ and $\mathbf{l}_8$ define in B0 a flat pencil of lines, $(\mathbf{l}_7\ \mathbf{l}_8)$, of G.
5) $\mathbf{l}_9 \in B0$, and based on the above theorem, $\mathbf{l}_9 \in G$ if and only if $\mathbf{l}_9 \in (\mathbf{l}_7\ \mathbf{l}_8)$.
6) If line $\mathbf{l}_3 \in G$ and $\mathbf{l}_9 \in g$, then $\mathbf{l}_6 \in G$ and vise-versa; if $\mathbf{l}_6 \in G$ and $\mathbf{l}_9 \in G$ then $\mathbf{l}_3 \in G \Rightarrow$ The condition for this singularity is

Singular configuration S1:

$${}^{\mathrm{P}}\mathrm{F}_{14} \cap {}^{\mathrm{P}}\mathrm{F}_{25} \cap {}^{\mathrm{P}}\mathrm{F}_{36} \cap \mathrm{B0} \neq \{\varnothing\}.$$

Note that this is Fichter's [38] singularity (5a), but in our case with the inversion of the equivalent mechanism, rotating the moving platform 90° about the vertical axis will not result in singular configuration.

2) Six Lines in a Special Linear Complex (5B): Since Γ includes three permanent flat pencils of type F, all its lines intersect a common line if this line is the line of intersection of planes ${}^{\mathrm{P}}\mathrm{F}_{14}$, ${}^{\mathrm{P}}\mathrm{F}_{25}$, and ${}^{\mathrm{P}}\mathrm{F}_{36}$ or if points $\mathbf{b}_1$, $\mathbf{b}_2$, and $\mathbf{b}_3$ are collinear. Since planes ${}^{\mathrm{P}}F_{14}$, ${}^{\mathrm{P}}F_{25}$, and ${}^{\mathrm{P}}F_{36}$ do not have a common intersection line the only possible singular configuration occurs when points $\mathbf{b}_1$, $\mathbf{b}_2$, and $\mathbf{b}_3$ are collinear (Fig. 7).

Singular configuration S2: $A\mathbf{b}_1 + B\mathbf{b}_2 + C\mathbf{b}_3 = 0$,

$$A, B, C \in \Re,\ (A, B, C) \neq (0, 0, 0).$$

This singularity is categorically the same (5b) as Hunt's [39] singularity, but co-planarity of one of the links with the moving

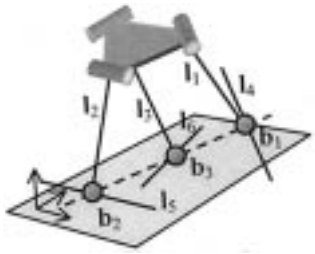

Fig. 7. S2 singularity.

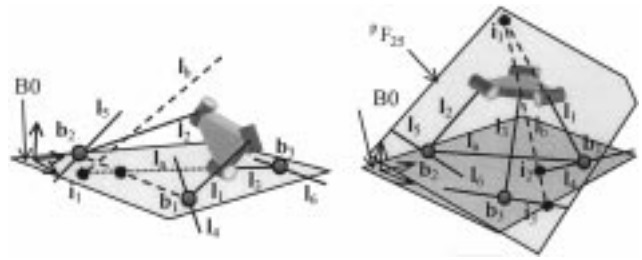

Fig. 8. (a) Special cases of S1 singularity: $\mathbf{l}_3 = \mathbf{l}_9$. (b) Special cases of S1 singularity: $\mathbf{l}_6 = \mathbf{l}_9$.

platform does not cause it as is the case with the Stewart–Gough 3-3 and 3-6 robots. Therefore, robots with such tripod may have better tilting capabilities than the Stewart–Gough 3-3 and 3-6 robots.

We will henceforth exclude the possibility for collinearity of $\mathbf{b}_1$, $\mathbf{b}_2$, and $\mathbf{b}_3$ since we already proved that this leads to a singular configuration.

B. Linear Congruence Singularities

This section presents the singularities of five lines in one linear congruence.

1) Elliptic Congruence (4A): Four skew lines in space form three distinct reguli and a fifth line linearly depends on them if it belongs to one of these reguli. Elliptic congruence singularities are not possible in our case since there are no four lines in the same regulus (see the proof in Section VI-C-1).

2) Hyperbolic Congruence (4B): Four lines concurrent with two other skew lines, $\mathbf{l}_\mathrm{a}$ and $\mathbf{l}_\mathrm{b}$, form a hyperbolic congruence. Any fifth line concurrent with $\mathbf{l}_\mathrm{a}$ and $\mathbf{l}_\mathrm{b}$ linearly depends on these four lines.

There are six line quintuplets in $\Gamma = \{\mathbf{l}_1 \ldots \mathbf{l}_6\}$ with two architectural flat pencils of type F in each quintuplet. Thus, line $\mathbf{l}_\mathrm{a}$ is defined by the centers of these flat pencils and line $\mathbf{l}_\mathrm{b}$ is the line of intersection between the two planes of these architectural flat pencils. Next, we prove that lines $\mathbf{l}_3$ or $\mathbf{l}_6$ intersect lines $\mathbf{l}_\mathrm{a}$ and $\mathbf{l}_\mathrm{b}$ only when the S1 and S2 singularities are formed.

There are two distinct categories of line quintuplets, G1 and G2. They are defined as

$$\mathrm{G1} = \{(\mathrm{l}_1\ \mathrm{l}_2\ \mathrm{l}_3\ \mathrm{l}_4\ \mathrm{l}_5), (\mathrm{l}_1\ \mathrm{l}_2\ \mathrm{l}_3\ \mathrm{l}_4\ \mathrm{l}_6), (\mathrm{l}_1\ \mathrm{l}_2\ \mathrm{l}_3\ \mathrm{l}_5\ \mathrm{l}_6)\}$$
$$\mathrm{G2} = \{(\mathrm{l}_1\ \mathrm{l}_2\ \mathrm{l}_4\ \mathrm{l}_5\ \mathrm{l}_6), (\mathrm{l}_1\ \mathrm{l}_3\ \mathrm{l}_4\ \mathrm{l}_5\ \mathrm{l}_6), (\mathrm{l}_2\ \mathrm{l}_3\ \mathrm{l}_4\ \mathrm{l}_5\ \mathrm{l}_6)\}.$$

The quintuplets $(\mathrm{l}_1\ \mathrm{l}_2\ \mathrm{l}_3\ \mathrm{l}_4\ \mathrm{l}_5)$ and $(\mathrm{l}_1\ \mathrm{l}_2\ \mathrm{l}_4\ \mathrm{l}_5\ \mathrm{l}_6)$ are used as category representing ones for G1 and G2, respectively. We first exclude the possibility that $\mathbf{b}_3 \in \mathrm{l}_\mathrm{a}$ since this clearly leads to singular configuration S2.

Proof:

1) $\mathrm{l}_\mathrm{a} = {}^\mathrm{c}\mathrm{F}_{14}{}^\mathrm{c}\mathrm{F}_{25}$, $\mathrm{l}_\mathrm{b} = {}^\mathrm{P}\mathrm{F}_{14} \cap {}^\mathrm{P}\mathrm{F}_{25}$.
2) $\mathbf{b}_1 = {}^\mathrm{c}F_{14}$, $\mathbf{b}_2 = {}^\mathrm{c}F_{25}$; therefore $\mathrm{l}_\mathrm{a} \in \mathrm{B0}$.
3) Lines l_6 and l_3 pass through $\mathbf{b}_3$.
4) Let $\mathbf{i}_1$ be the piercing point of l_b with B0.
5) Lines l_6 and l_3 intersect l_a only if they lie in B0.
6) Lines l_6 and l_3 intersect both lines l_a and l_b only if they pass through point $\mathbf{i}_1$ and lie in the base plane B0.
7) In such a case, lines l_7 and l_8 are, respectively, defined by points $\mathbf{b}_1$ and $\mathbf{i}_1$ and $\mathbf{b}_2$ and $\mathbf{i}_1$. Line l_9 is defined by point $\mathbf{b}_3$ and $\mathbf{i}_1$. This shows that lines l_7, l_8, and l_9 intersect in one point, $\mathbf{i}_1$, in B0. Fig. 8(a) shows the case when line l_9 is l_3 and Fig. 8(b) shows the case $\mathrm{l}_6 = \mathrm{l}_9$. Both these cases are special cases of S1.

3) Parabolic Congruence (4C): This case unifies all flat pencil singularities related with one or more flat pencils of the parabolic congruence, therefore, it does not add new singular configurations to the ones that will be discussed in flat pencil singularities.

4) Degenerate Congruence (4D): The lines dependent on four generators of a degenerate congruence are the lines of a plane (3D) and the lines that share the piercing point of the fourth congruence line with the congruence plane. Since co-planarity of four lines will be investigated in Section VI-C-4 (3D), we inspect only the case in which two lines pierce the plane defined by the other three lines in a common point. However, if the considered line triplet is coplanar only when four or more lines of Γ are coplanar, then degenerate congruence singularity is marked.

Γ has 20 line triplets. Table II lists all these line triplets and presents six groups of them, U1 ... U6. We consider all the cases in which these line triples are coplanar and two other lines intersect their plane in a common point.

Case 1: U1 Line Triples: This category includes only one line triplet, $(\mathrm{l}_1, \mathrm{l}_2, \mathrm{l}_3)$. Next, we prove that this line triplet is coplanar only when the moving platform lies in the tripod base plane and that in this case l_1, l_2, and l_3 belong to one flat pencil (Fig. 9).

Proof:

1) Points $\mathbf{p}_i$ and $\mathbf{b}_i$ define line l_i, and P0, $i = 1 \ldots 3$.
2) Points $\mathbf{b}_i$ define B0.
3) $\mathrm{l}_i \in \mathrm{Pi}$, $n = \mathrm{P1} \cap \mathrm{P2} \cap \mathrm{P3}$.
4) Since $\mathrm{P0} = \mathrm{B0}$ then lines l_1, l_2, and l_3 lie in B0 and intersect in the piercing point of $\mathbf{n}$ with B0. Hence, lines l_1, l_2, and l_3 belong to one flat pencil (Fig. 9).

This singularity is named singular configuration S3.

$$\text{Singular configuration S3: } \mathrm{B0} = \mathrm{P0} \Rightarrow \mathrm{l}_n \in \mathrm{T}_{jk},$$
$$j, k, n = 1, 2, 3, \quad j \neq k \neq n.$$

We will henceforth exclude the possibility that the moving platform lies in the tripod base plane since we already showed that this configuration is singular.

Case 2: U2 Line Triplets: Let $(\mathrm{l}_1\ \mathrm{l}_3\ \mathrm{l}_5)$ be a category-representing triplet. We assume that lines $(\mathrm{l}_1\ \mathrm{l}_3\ \mathrm{l}_5)$ are coplanar, thus, lines l_1 and l_3 define the flat pencil ${}^\mathrm{P}\mathrm{T}_{13}$. There are two cases to be considered, in which, the line pairs $(\mathrm{l}_4\ \mathrm{l}_6)$ and $(\mathrm{l}_2\ \mathrm{l}_6)$, respectively, intersect ${}^\mathrm{P}T_{13}$ in a single point. Lines l_4, l_2, and l_6 pierce ${}^\mathrm{P}\mathrm{T}_{13}$ in points $\mathbf{b}_1$, $\mathbf{b}_2$, and $\mathbf{b}_3$, respectively. Accordingly, intersection of two lines out of l_4, l_2, and l_6 with ${}^\mathrm{P}\mathrm{T}_{13}$ in one point

TABLE II
ALL 20 LINE-TRIPLES DIVIDED INTO SIX GROUPS

U1 = {(l_1 l_2 l_3)}
U2 = {(l_1 l_3 l_5), (l_2 l_3 l_4), (l_1 l_2 l_6)}
U3 = {(l_1 l_2 l_4), (l_1 l_2 l_5), (l_1 l_3 l_5), (l_1 l_3 l_6), (l_2 l_3 l_5), (l_2 l_3 l_6)}
U4 = {(l_1 l_4 l_5), (l_1 l_4 l_6), (l_2 l_5 l_6), (l_3 l_5 l_6), (l_3 l_4 l_6), (l_2 l_4 l_5)}
U5 = {(l_1 l_5 l_6), (l_2 l_4 l_6), (l_3 l_4 l_5)}
U6 ={(l_4 l_5 l_6)}

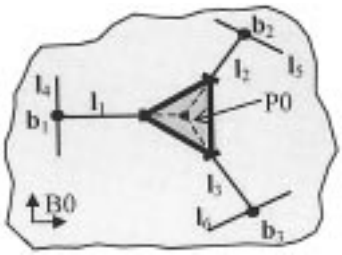

Fig. 9. Singularity of type S3.

is possible only if two spherical joints coincide, i.e., $\mathbf{b}_i = \mathbf{b}_j$, $i, j = 1, 2, 3$; $i \neq j$. This configuration is a special case of S2 (Fig. 7).

Case 3: U3 Line Triples: All the line triplets in this category include one flat pencil of type F. Let $(\mathrm{l}_1 \mathrm{l}_2 \mathrm{l}_4)$ be a category-representing line triplet. We assume that the lines of this triplet are coplanar and we examine the other lines. This examination leads to a special case of S1 singularity (Fig. 10). In this configuration lines l_7, l_8, and l_9 intersect in one common point in B0.

Proof:

1) Lines $\mathbf{r}_1$ and $\mathbf{p}_1\mathbf{p}_2$ are the intersection lines of ${}^{\mathrm{P}}\mathrm{F}_{14}$ and ${}^{\mathrm{P}}\mathrm{T}_{12}$ with P0, respectively.
2) ${}^{\mathrm{P}}\mathrm{T}_{12} = {}^{\mathrm{P}}\mathrm{F}_{14}$ when lines $(\mathrm{l}_1\ \mathrm{l}_2\ \mathrm{l}_4)$ are coplanar.
3) Since lines $\mathbf{r}_1$ and $\mathbf{p}_1\mathbf{p}_2$ are distinct and coplanar, they define the platform plane P0.
4) For ${}^{\mathrm{P}}\mathrm{T}_{12} = {}^{\mathrm{P}}\mathrm{F}_{14}$ to be fulfilled then both lines $\mathbf{r}_1$ and $\mathbf{p}_1\mathbf{p}_2$ must belong to both ${}^{\mathrm{P}}\mathbf{T}_{12}$ and ${}^{\mathrm{P}}\mathrm{F}_{14}$. Thus, this is achieved only when ${}^{\mathrm{P}}\mathrm{T}_{12} = {}^{\mathrm{P}}\mathrm{F}_{14} = \mathrm{P0}$.
5) Since $\mathrm{l}_5 \parallel \mathrm{P0}$ and $\mathbf{b}_2 \in \mathrm{l}_5 \Rightarrow \mathrm{l}_5 \in \mathrm{P0}$. Thus, the four lines l_1, l_2, l_4, l_5 are coplanar (see Fig. 10).

In this configuration lines l_7, l_8, and l_9 intersect in one common point in B0 resulting in a special case of S1.

Case 4: U4 Line Triples: Let $(\mathrm{l}_1, \mathrm{l}_4, \mathrm{l}_5)$ line triplet be a category representing one. Using similar arguments as in the previous case, this line triplet is coplanar only if all its lines lie in the moving platform plane, P0, i.e., ${}^{\mathrm{P}}\mathrm{S}_{45} = {}^{\mathrm{P}}\mathrm{F}_{14} = \mathrm{P0}$. In this case line l_2 lies in P0 since it is defined by point $\mathbf{b}_2 \in \mathrm{l}_5$ and $\mathbf{p}_2 \in \mathrm{P0}$. This is the singular configuration of Fig. 10.

Case 5: U5 Line Triples: This case leads to singular configuration S3. Next, we assume that the lines in the category representing line triplet $(\mathrm{l}_3, \mathrm{l}_4, \mathrm{l}_5)$ are coplanar and we show that this occurs only if the $\mathrm{P0} = \mathrm{B0}$ (S3 singularity in Fig. 9).

Proof:

1) $\mathrm{l}_4 \parallel \mathrm{P0}$ $\mathrm{l}_5 \parallel \mathrm{P0}$ [corollary Cr2] therefore ${}^{\mathrm{P}}\mathrm{S}_{45} \parallel \mathrm{P0}$.
2) Point $\mathbf{p}_3$ satisfies: $\mathbf{p}_3 \in \mathrm{P0}$, $\mathbf{p}_3 \in \mathrm{l}_3$.
3) $\mathrm{l}_3 \in {}^{\mathrm{P}}\mathrm{S}_{45} \Rightarrow \mathbf{p}_3 \in {}^{\mathrm{P}}\mathrm{S}_{45} \Rightarrow {}^{\mathrm{P}}\mathrm{S}_{45} = \mathrm{P0}$.

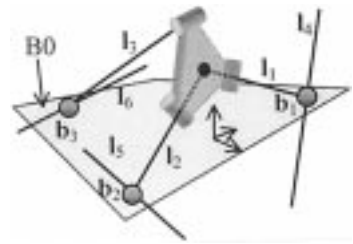

Fig. 10. Special case of S1.

4) Point $\mathbf{b}_3$ lies on l_3, i.e., $\mathbf{b}_3 \in \mathrm{l}_3$, and $\mathbf{b}_3 \in {}^{\mathrm{P}}\mathrm{S}_{45}$.
5) Points $\mathbf{b}_1$ and $\mathbf{b}_2$ satisfy: $\mathbf{b}_1 \in \mathrm{l}_4$, $\mathbf{b}_2 \in \mathrm{l}_5$; hence $\mathbf{b}_1 \in {}^{\mathrm{P}}\mathrm{S}_{45}$ and $\mathbf{b}_2 \in {}^{\mathrm{P}}\mathrm{S}_{45}$.
6) $\mathrm{B0} = {}^{\mathrm{P}}\mathrm{S}_{45} = \mathrm{P0}$ since $\mathbf{b}_1$, $\mathbf{b}_2$, and $\mathbf{b}_3$ belong to ${}^{\mathrm{P}}\mathrm{S}_{45}$.

Case 6: U6 Line Triples: Lines $(\mathrm{l}_4, \mathrm{l}_5, \mathrm{l}_6)$ are coplanar if the moving platform and the tripod base plane are parallel one to another. Excluding the case $\mathrm{P0} = \mathrm{B0}$, two lines from the group $(\mathrm{l}_1, \mathrm{l}_2, \mathrm{l}_3)$ intersect the tripod base plane in a common point only if two of the spherical joints coincide. This leads to a special case of singular configuration S2 in Fig. 7.

Proof:

1) Lines l_1, l_2, l_3 pierce the base plane in points $\mathbf{b}_1$, $\mathbf{b}_2$, and $\mathbf{b}_3$, respectively.
2) $\mathrm{l}_4 \parallel \mathrm{P0}$ $\mathrm{l}_5 \parallel \mathrm{P0}$ $\mathrm{l}_6 \parallel \mathrm{P0}$ [corollary Cr2]. In a singular configuration two lines out of l_1, l_2, l_3 pierce the base plane in a common point. Therefore, in such singular configuration $\mathbf{b}_i = \mathbf{b}_j$, $i = 1, 2, 3$, $i \neq j$.

C. Planes Singularities

This section presents the analysis of singularities that belong to a rank-three system. We inspect all the cases, in which, four lines belong to the planes variety.

1) Regulus Singularities (3A): The group of lines Γ includes three architectural flat pencils F_{14}, F_{25}, and F_{36}. Consequently, the maximal number of skew lines in Γ is three. We recall that all lines in the same regulus are skew and intersect all the lines in the conjugate regulus [30]. Therefore, if lines l_1, l_2, l_3 form a regulus, then lines l_4, l_5, and l_6 cannot belong to this regulus because line l_4 intersects l_1, l_5 intersects l_2, and l_6 intersects l_3. Consequently, no group of more than three lines can belong to the same regulus and singularity of type (3A) is not possible.

2) Union Singularities (3B): The lines that depend on the generators of a union are all the lines that depend on any of its two flat pencils. Therefore, this case does not add singularities to the ones that stem from flat pencil singularities.

3) Bundle Singularities (3C): A bundle that is singular includes more than three lines intersecting in a common point. In order to find all singular bundles in Γ, all the possible line quadruplets are registered and divided into four line quadruplet groups.

Table III lists all the 15 line quadruplets. A singular bundle forms if all the lines of one of these line quadruplets are copunctal. This table presents four different quadruplet groups, namely, groups Q1, Q2, Q3, and Q4.

Case 1: Singularities of Q1 Line Quadruplets: This case leads to special cases of S1 singularity in which the six lines of Γ or the four lines $(\mathrm{l}_1\ \mathrm{l}_2\ \mathrm{l}_3\ \mathrm{l}_6)$ belong to one bundle (Fig. 11(a)

TABLE III
15-LINE QUADRUPLETS IN FOUR DIFFERENT CATEGORIES

Q1 = {(l_1 l_2 l_3 l_4), (l_1 l_2 l_3 l_5), (l_1 l_2 l_3 l_6)}	Q3 = {(l_1 l_2 l_4 l_6), (l_1 l_3 l_4 l_5), (l_2 l_3 l_4 l_5), (l_1 l_2 l_5 l_6), (l_1 l_3 l_5 l_6), (l_2 l_3 l_4 l_6)}.
Q2 = {(l_1 l_2 l_4 l_5), (l_1 l_3 l_4 l_6), (l_2 l_3 l_5 l_6)}	Q4 = {(l_1 l_4 l_5 l_6), (l_2 l_5 l_4 l_6), (l_3 l_6 l_4 l_5)}

and (b), respectively). We choose $(\mathrm{l}_1\ \mathrm{l}_2\ \mathrm{l}_3\ \mathrm{l}_6)$ as a category representing line quadruplet.

Proof:

1) Point $\mathbf{b}_3$ fulfills $\mathbf{b}_3 = \mathrm{l}_3 \cap \mathrm{l}_6$, i.e., $\mathbf{b}_3 = {}^{\mathrm{c}}\mathrm{F}_{36}$.
2) In a singular configuration, lines l_1, l_2, l_3, and l_6 intersect in one common point.
3) Since $\mathbf{b}_3 = \mathrm{l}_3 \cap \mathrm{l}_6$ and $\mathrm{l}_3 \neq \mathrm{l}_6$ the only possible common point of intersection for lines l_1, l_2, l_3, and l_6 is $\mathbf{b}_3$.
4) $\mathbf{b}_3 \in \mathrm{l}_3$, $\mathrm{l}_3 \in \mathrm{P3}$, $\mathrm{l}_2 \in \mathrm{P2}$, and $\mathrm{l}_1 \in \mathrm{P1}$; therefore, the intersection is possible only along the normal $\mathbf{n} = \mathrm{P1} \cap \mathrm{P2} \cap \mathrm{P3}$, i.e., $\mathbf{b}_3 \in \mathbf{n}$.
5) $\mathbf{b}_3 \in \mathrm{B0}$ and in a singular configuration $\mathbf{b}_3 \in \mathbf{n}$; therefore, $\mathbf{b}_3 = \mathbf{n} \cap \mathrm{B0}$, namely, $\mathbf{b}_3$ is the piercing point of $\mathbf{n}$ with the tripod base plane B0.
6) In a singular configuration ${}^{\mathrm{c}}\mathrm{T}_{12} = {}^{\mathrm{c}}\mathrm{F}_{36} = \mathbf{b}_3$. Therefore, there are two possibilities: ${}^{\mathrm{c}}\mathrm{T}_{12}$ is located above the moving platform and ${}^{\mathrm{c}}\mathrm{T}_{12}$ is located beneath the moving platform.
7) If ${}^{\mathrm{c}}\mathrm{T}_{12}$ is beneath the moving platform it means that $\mathbf{b}_1 = \mathbf{b}_2 = \mathbf{b}_3$; therefore, this is a special case of S1 singularity [Fig. 11(a).]

If ${}^{\mathrm{c}}\mathrm{T}_{12}$ is above the moving platform then $\mathrm{l}_1 = \mathbf{b}_1\mathbf{b}_3$ and $\mathrm{l}_2 = \mathbf{b}_2\mathbf{b}_3$, therefore, $\mathrm{l}_1 \in \mathrm{B0}$, $\mathrm{l}_2 \in \mathrm{B0}$. This singularity is a special case of S1, Fig. 11(b).

Case 2: Singularities of Q2 Line Quadruplets: Let $(\mathrm{l}_1\ \mathrm{l}_2\ \mathrm{l}_4\ \mathrm{l}_5)$ be a category representing line quadruplet. This line quadruplet forms a singular bundle if a pair of spherical joints coincides.

Proof: $\mathbf{b}_1 = \mathrm{l}_1 \cap \mathrm{l}_4$, $\mathbf{b}_2 = \mathrm{l}_2 \cap \mathrm{l}_5$. The only possible intersection point for the four distinct lines is $\mathbf{b}_1 = \mathbf{b}_2$. Hence, this is the same special case of S2 singularity in Fig. 7.

Case 3: Singularities of Q3 Lines Quadruplets: Let $(\mathrm{l}_1\ \mathrm{l}_2\ \mathrm{l}_4\ \mathrm{l}_6)$ be a category-representing quadruplet. Next, we assume that this line quadruplet intersects in one point and we show that singularity of this category is a special case of singular configuration S2.

Proof:

1) Point $\mathbf{b}_1$ fulfills $\mathbf{b}_1 \in \mathrm{B0}$, $\mathbf{b}_1 = \mathrm{l}_1 \cap \mathrm{l}_4$; therefore, in a singular configuration lines l_1, l_2, l_4, and l_6 intersect in point $\mathbf{b}_1$.
2) $\mathrm{l}_1 \in \mathrm{P1}$, $\mathrm{l}_2 \in \mathrm{P2}$; thus, the intersection points of these lines is located along $\mathbf{n} = \mathrm{P1} \cap \mathrm{P2}$.
3) In a singular configuration line l_2 intersects l_1 in point $\mathbf{b}_1$. Hence, $\mathbf{b}_1 = {}^{\mathrm{c}}\mathrm{T}_{12}$.
4) $\mathbf{b}_2 = \mathrm{l}_2 \cap \mathrm{B0}$, i.e., $\mathbf{b}_2$ is the piercing point of l_2 with the tripod base plane. Therefore $\mathbf{b}_1 = \mathbf{b}_2 = {}^{\mathrm{c}}\mathrm{T}_{12}$ and this is the same special case of S2 shown in Fig. 7.

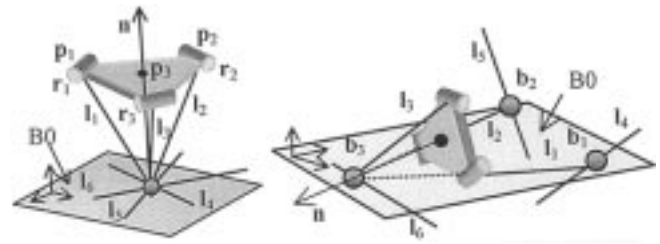

Fig. 11. Special cases of S1 singularity.

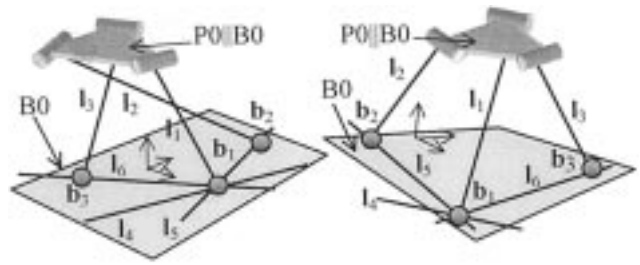

Fig. 12. Special cases of S1 singularity.

Case 4: Singularities of Q4 Lines Quadruplets: Let $(\mathrm{l}_1\ \mathrm{l}_4\ \mathrm{l}_5\ \mathrm{l}_6)$ be a category-representing quadruplet. This case leads to two special cases of S1 singularity (Fig. 12).

Proof:

1) $\mathbf{b}_1 = \mathrm{l}_1 \cap \mathrm{l}_4$; therefore, in a singular configuration, $\mathbf{b}_1$ is the common intersection point of all lines in the quadruplet.
2) $\mathrm{l}_6 \parallel \mathrm{P0}$, $\mathrm{l}_5 \parallel \mathrm{P0}$ [corollary Cr2]; thus, ${}^{\mathrm{P}}\mathrm{S}_{56} \parallel \mathrm{P0}$.
3) $\mathbf{b}_1 \in \mathrm{B0}$ and in singular a configuration $\mathbf{b}_1 = {}^{\mathrm{c}}\mathrm{S}_{56}$; therefore, ${}^{\mathrm{c}}\mathrm{S}_{56} \in \mathrm{B0}$.

Points $\mathbf{b}_2$, $\mathbf{b}_3$, and ${}^{\mathrm{c}}\mathrm{S}_{56}$ define ${}^{\mathrm{P}}\mathrm{S}_{56}$. Since all these points belong to B0, we conclude that in a singular configuration $\mathrm{B0} \parallel \mathrm{P0}$, i.e., the tripod base plane and the moving platform are parallel. Fig. 12 presents the two special cases of singular configurations S1.

4) Plane Singularities (3D): Singularities of type 3D are characterized by having more than three coplanar lines in the group $\Gamma = \{\mathrm{l}_1, \mathrm{l}_2, \mathrm{l}_3, \mathrm{l}_4, \mathrm{l}_5, \mathrm{l}_6\}$. We inspect all the line quadruplets to determine the singularities that stem from this case. There are four line quadruplet groups as shown in Table III; therefore, we consider the cases, in which, the lines of each category-representing quadruplet are coplanar.

Case 1: Q1 Coplanar Line Quadruplet: All line quadruplets in this group include lines l_1, l_2, and l_3. We proved in Section VI-B-IV Case 1 that lines $\mathrm{l}_1\ \mathrm{l}_2\ \mathrm{l}_3$ are coplanar only if $\mathrm{B0} = \mathrm{P0}$ leading to S3 singularity.

Case 2: Q2 Coplanar Line Quadruplet: Let $(\mathrm{l}_1\ \mathrm{l}_2\ \mathrm{l}_4\ \mathrm{l}_5)$ be a category representing line quadruplet. In Section VI-B-IV, Case 3, we proved that the lines of this quadruplet are coplanar only when lines l_1 and l_2 lie in P0 leading to the special case of S1 singularity in Fig. 10.

Case 3: Q3 Coplanar Line Quadruplet: Choose $(\mathrm{l}_1\ \mathrm{l}_2\ \mathrm{l}_4\ \mathrm{l}_6)$ as a category-representing quadruplet. All quadruplets of this category are coplanar only if $\mathrm{P0} = \mathrm{B0}$.

Proof:

1) In a singular configuration, the coplanar lines $\mathrm{l}_4 \parallel \mathrm{P0}$ and $\mathrm{l}_6 \parallel \mathrm{P0}$ define a plane ${}^{\mathrm{P}}\mathrm{S}_{46}$ such that ${}^{\mathrm{P}}\mathrm{S}_{46} \parallel \mathrm{P0}$.

2) Point $\mathbf{p}_1$ fulfills $\mathbf{p}_1 \in \mathbf{l}_1$, $\mathbf{p}_1 \in \mathrm{P0}$. Point $\mathbf{b}_1$ is the piercing point of $\mathbf{l}_1$ with ${}^{\mathrm{P}}\mathrm{S}_{46}$, $\mathbf{b}_1 = \mathbf{l}_1 \cap {}^{\mathrm{P}}\mathrm{S}_{46}$. Accordingly, the condition to fulfill $\mathbf{l}_1 \in {}^{\mathrm{P}}\mathrm{S}_{46}$ is ${}^{\mathrm{P}}\mathrm{S}_{46} = \mathrm{P0}$.
3) Point $\mathbf{p}_2$ fulfills $\mathbf{p}_2 \in \mathrm{P0}$, therefore $\mathbf{l}_2 \in {}^{\mathrm{P}}\mathrm{S}_{46}$ when $\mathbf{b}_2 \in \mathrm{P0}$. This configuration is S3 singularity (Fig. 9).

Case 4: Q4 Coplanar Line Quadruplet: Let $(\mathbf{l}_1\ \mathbf{l}_4\ \mathbf{l}_5\ \mathbf{l}_6)$ be a category-representing line quadruplet. Based on the proof in Case 3, all the lines of this quadruplet are coplanar if $\mathrm{P0} = \mathrm{B0}$.

D. Flat Pencil Singularities (2B)

In the following sections, a category representing flat pencil defined by lines $\mathbf{l}_j$ and $\mathbf{l}_k$ $(\mathbf{l}_j, \mathbf{l}_k \in \Gamma)$ is tested with each line $\mathbf{l}_n$ in the complementary group C_{jk}. The geometric relations that render $\mathbf{l}_n \in$ flat-pencil $(\mathbf{l}_j, \mathbf{l}_k)$ are considered.

Case 1: Line $\mathbf{l}_n \in T_{jk}, j,k = 1,2,3, j \neq k, \mathbf{l}_n \in \mathrm{C}_{jk}$*:* Let T_{12} be a category representing flat pencil. Based on the symmetry of the tripod, there are three distinct cases: $\mathbf{l}_n = \mathbf{l}_3$, $\mathbf{l}_n = \mathbf{l}_4$, and $\mathbf{l}_n = \mathbf{l}_6$. The case $\mathbf{l}_n = \mathbf{l}_5$ is equivalent to case $\mathbf{l}_n = \mathbf{l}_4$ due to symmetry considerations.

Case 1.1 $\mathbf{l}_n = \mathbf{l}_3$: This case was investigated in Section VI-B-4, Case 1.

Case 1.2 $\mathbf{l}_n = \mathbf{l}_4$ (equivalent to $\mathbf{l}_n = \mathbf{l}_5$): Section VI-B-4, Case 3, shows that if $\mathbf{l}_1$, $\mathbf{l}_2$ and $\mathbf{l}_4$ are coplanar then the singular configuration in Fig. 10 forms.

Case 1.3 $\mathbf{l}_n = \mathbf{l}_6$: This case is a special case of Section VI-C-3, Case 1 limited for an equilateral-triangular moving platform. Using similar arguments, it is possible to see that this leads to the singularity of Fig. 11 with lines $\mathbf{l}_6\,\mathbf{l}_1$ and $\mathbf{l}_2$ that belong to one flat pencil. Note that an equilateral triangular moving platform fulfills $\mathbf{r}_3 \parallel \mathbf{p}_1\mathbf{p}_2$, and $\mathbf{l}_6 \parallel \mathbf{p}_1\mathbf{p}_2$.

Case 2: Line $\mathbf{l}_n \in \mathrm{F}_{jk}, (j,k) \in \{(1,4),(2,5),(3,6)\}, \mathbf{l}_n \in \mathrm{C}_{jk}$*:* Let F_{14} be a category representing flat pencil. Based on the symmetry of the tripod, we consider only two cases: $\mathbf{l}_n = \mathbf{l}_2$ (equivalent to $\mathbf{l}_n = \mathbf{l}_3$) and $\mathbf{l}_n = \mathbf{l}_5$ (equivalent to $\mathbf{l}_n = \mathbf{l}_6$).

Case 2.1 $\mathbf{l}_n = \mathbf{l}_2$ (equivalent to $\mathbf{l}_n = \mathbf{l}_3$): This case is identical to Case 1.2 $\mathbf{l}_n = \mathbf{l}_4$.

Case 2.2 $\mathbf{l}_n = \mathbf{l}_5$ (equivalent to $\mathbf{l}_n = \mathbf{l}_6$): In Section VI-B-4, Case 4, we proved that if lines $\mathbf{l}_1$, $\mathbf{l}_4$, and $\mathbf{l}_5$ are coplanar then the singular configuration in Fig. 10 forms.

Case 3: Line $\mathbf{l}_n \in \mathrm{S}_{jk}, (j,k) \in \{(4,5),(4,6),(5,6)\}, \mathbf{l}_n \in \mathrm{C}_{jk}$*:* Let S_{45} be a category representing flat pencil. There are three distinct cases to be considered: $\mathbf{l}_n = \mathbf{l}_1$ (analogous to $\mathbf{l}_n = \mathbf{l}_2$), $\mathbf{l}_n = \mathbf{l}_3$, and $\mathbf{l}_n = \mathbf{l}_6$.

Case 3.1 $\mathbf{l}_n = \mathbf{l}_1$ (equivalent to $\mathbf{l}_n = \mathbf{l}_2$): Same as Case 2.2.

Case 3.2 $\mathbf{l}_n = \mathbf{l}_3$: In Section VI-B-4, Case 5, we proved that if lines $\mathbf{l}_3$, $\mathbf{l}_4$, and $\mathbf{l}_5$ are coplanar then S3 singularity forms.

Case 3.3 $\mathbf{l}_n = \mathbf{l}_6$: This case leads to a special case of S1 singularity (Fig. 13).

Proof:

1) $\mathbf{l}_4 \parallel \mathrm{P0}$ $\mathbf{l}_5 \parallel \mathrm{P0}$ (corollary Cr2) therefore ${}^{\mathrm{P}}\mathrm{S}_{45} \parallel \mathrm{P0}$.
2) In a singular configuration $\mathbf{l}_6 \in {}^{\mathrm{P}}\mathrm{S}_{45}$ and ${}^{\mathrm{P}}\mathrm{S}_{45} \in \mathbf{l}_6$.
3) $\mathbf{b}_1 \in \mathbf{l}_4$, $\mathbf{b}_2 \in \mathbf{l}_5$ and $\mathbf{b}_3 \in \mathbf{l}_6$; therefore $\mathbf{b}_1 \in {}^{\mathrm{c}}\mathrm{S}_{45}$, $\mathbf{b}_2 \in {}^{\mathrm{P}}\mathrm{S}_{45}$, $\mathbf{b}_3 \in {}^{\mathrm{P}}\mathrm{S}_{45}$ and plane B0 fulfills $\mathrm{B0} = {}^{\mathrm{P}}\mathrm{S}_{45} \parallel \mathrm{P0}$. The special cases of singular configuration S1 are illustrated in Fig. 13.

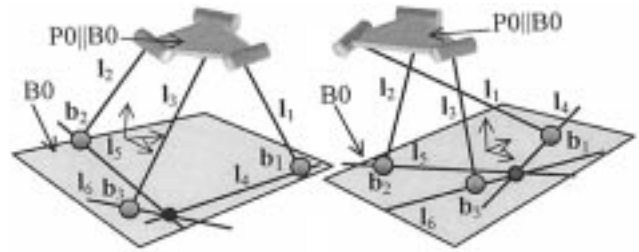

Fig. 13. Special cases of S1 singularity.

TABLE IV
SUBCASES OF CASE 4 AND THEIR EQUIVALENT CASES

case:	$\mathbf{l}_n = \mathbf{l}_2$	$\mathbf{l}_n = \mathbf{l}_3$	$\mathbf{l}_n = \mathbf{l}_4$	$\mathbf{l}_n = \mathbf{l}_6$
Equal to:	case 1.2	case 1.3	case 2.2	case 3.2

Case 4 $\mathbf{l}_n \in \mathrm{R}_{jk}, (j,k) \in \{(1,5),(1,6),(2,4),(2,5),(3,4),(3,5)\}$, $\mathbf{l}_n \in \mathrm{C}_{jk}$*:* Let R_{15} be a category representing flat pencil. This case leads to four cases that we have already dealt with, Table IV.

E. Point Singularities (1A)

Given the perpendicularity relation in Cr4, a line of $\{\mathbf{l}_1, \mathbf{l}_2, \mathbf{l}_3\}$ does not coincide with a line of $\{\mathbf{l}_4, \mathbf{l}_5, \mathbf{l}_6\}$. Lines $\mathbf{l}_1$, $\mathbf{l}_2$, and $\mathbf{l}_3$ belong to three distinct planes P1, P2, and P3, and they pass through three distinct points $\mathbf{p}_1$, $\mathbf{p}_2$, and $\mathbf{p}_3$. Consequently, no line couple from these lines can be simultaneously concurrent with the intersection line of the three planes P1, P2, and P3. This precludes the coincidence of a line-pair of $\{\mathbf{l}_1, \mathbf{l}_2, \mathbf{l}_3\}$.

Lines $\mathbf{l}_4$, $\mathbf{l}_5$, $\mathbf{l}_6$ move such that each one is perpendicular to planes P1, P2, P3, respectively. Since these planes are distinct, any two lines of this group cannot coincide regardless of the configuration of the robot.

Based on the above arguments, we conclude that the point singularity of the tripod of Fig. 4 is not possible because the lines of Γ are architecturally distinct (regardless of the robot configuration).

This completes the analysis of the parallel singularities that characterize the family of composite serial in-parallel robots of Table I. To complete the singularity analysis for each robot in this table, one should find the serial singularities stemming from singularities of the IIK matrix of each robot. The serial singularities of the RSPR and the USR robots were analyzed in [27] based on their IIK matrices [24].

The results of the analysis of the parallel singularities indicate that there are three general parallel singularities, S1, S2, and S3, all of which are connected to the general complex singularity. Parallel singularities of lower rank were identified as special cases of S1, S2, and S3.

VII. CONCLUSION

This paper presented the analysis of the parallel singularities of a class of 14 composite serial in-parallel robots having a common tripod mechanism. A unified Jacobian formulation

of this class of robots was achieved by formulating a line-based Jacobian matrix of the tripod mechanism (called here as the common parallel submechanism), which is an inversion of the equivalent mechanism of the Stewart–Gough 3-3 and 3-6 robots. This line-based formulation provides a convenient method for analyzing the parallel singularities of this class of robots utilizing line geometry.

The analysis revealed three general cases (that are in fact special cases of the general complex singularity) of parallel singularities that are common to this family of robots. All other singular configurations were shown to be special cases of the general complex.

Even though this family of robots suffers also from Hunt's [1], [39], [40] and Fichter's [38] singularities, which are typical of 3-3 and 3-6 Stewart–Gough platforms; nevertheless, they have different interpretation in its working capabilities. It has been shown that rotation of the moving platform by 90° about the Z axis which leads to Fichter's singularity in the Stewart–Gough 3-6 and 3-3 platforms, or aligning one of the links with the moving platform plane which leads to Hunt's singularity, does not correspond to parallel singularity of the robots of this family.

This geometrically-based analysis of parallel singularities, complemented by serial singularity analysis and a comparison between the USR and the RSPR robots [27], was an important factor in the design and construction of a compact and a lightweight RSPR robot for medical applications.

REFERENCES

[1] J. P. Merlet, "Singular configurations of parallel manipulators and Grassmann geometry," *Int. J. Robot. Res.*, vol. 8, no. 5, 1989.

[2] C. Gosselin and J. Angeles, "Singularity analysis of closed-loop kinematic chains," *IEEE Trans. Robot. Automat.*, vol. 6, pp. 281–290, June 1990.

[3] K. H. Hunt, A. E. Samuel, and P. R. McAree, "Special configurations of multi-finger multi-freedom grippers—A kinematic study," *Int. J. Robot. Res.*, vol. 10, no. 2, pp. 123–134, 1991.

[4] O. Ma and J. Angeles, "Architecture singularities of parallel manipulators," *IEEE Trans. Robot. Automat.*, vol. 7, no. 1, pp. 23–29, 1992.

[5] D. Zlatanov, R. G. Fenton, and B. Benhabib, "A unifying framework for classification and interpretation of mechanism singularities," *ASME J. Mech. Des.*, vol. 117, pp. 566–572, 1995.

[6] D. Basu and A. Ghosal, "Singularity analysis of platform-type multi-loop spatial mechanisms," *Mech. Mach. Theory*, vol. 32, no. 3, pp. 375–389, 1997.

[7] R. Ben-Horin, "Criteria for Analysis of Parallel Robots," Ph.D. dissertation, Technion, Haifa, Israel, 1997.

[8] L. Notash, "Uncertainty configurations of parallel manipulators," *Mech. Mach. Theory*, vol. 33, no. 1, pp. 123–138, 1998.

[9] F. C. Park and J. W. Kim, "Singularity analysis of closed kinematic chains," *J. Mech. Des.*, vol. 121, no. 1, 1999.

[10] D. Chablat and Ph. Wenger, "Working modes and aspects in fully parallel manipulators," in *IEEE Int. Conf. Robotics and Automation*, 1998, pp. 1964–1969.

[11] L.-W. Tsai, *Robot Analysis the Mechanics of Serial and Parallel Manipulators*. New York: Wiley, 1999.

[12] K. H. Hunt, *Kinematic Geometry of Mechanisms*. Oxford, U.K.: Clarendon, 1978.

[13] F. Hao and J. M. McCarthy, "Conditions for line-based singularities in spatial platform manipulators," *J. Robot. Syst.*, vol. 15, no. 1, pp. 43–55, 1998.

[14] A. Dandurand, "The rigidity of compound spatial grid," *Structural Topol.*, vol. 10, pp. 41–56, 1984.

[15] C. L. Collins and G. L. Long, "The singularity analysis of an in-parallel hand controller for force-reflected teleoperation," *IEEE Trans. Robot. Automat.*, vol. 11, pp. 661–669, Oct. 1995.

[16] L. Notash and R. Podhorodeski, "Forward displacement analysis and uncertainty configurations of parallel manipulators with a redundant branch," *J. Robot. Syst.*, vol. 13, no. 9, pp. 587–601, 1996.

[17] D. Zlatanov, M. Q. Dai, R. G. Fenton, and B. Benhabib, "Mechanical design and kinematic analysis of a three-legged six degree-of-freedom parallel manipulator," in *Robotics, Spatial Mechanisms, and Mechanical Systems*: ASME, 1992, vol. DE-45, pp. 529–536.

[18] M. Ceccarelli, "A study of feasibility for a new wrist," in *Proc. World Automation Congress (WAC'96)*, vol. 3, 1996, pp. 161–166.

[19] M. Soreli, C. Ferraresi, M. Kolarski, C. Borovac, and M. Vukobratovic, "Mechanics of Turin parallel robot," *Mech. Mach. Theory*, vol. 32, no. 1, pp. 51–77, 1997.

[20] Y. K. Byun and H. S. Cho, "Analysis of a novel 6-DOF, 3-PPSP parallel manipulator," *Int. J. Robot. Res.*, vol. 16, no. 6, pp. 859–872, 1997.

[21] F. Tahmasebi and L.-W. Tsai, "Workspace and singularity analysis of novel six-DOF parallel minimanipulator," ISR Tech. Res. Rep., T. R. 93-55, 1993.

[22] L. -W. Tsai, "The Jacobian Analysis of Parallel Manipulators Using Reciprocal Screws," in *Advances in Robot Kinematics: Analysis and Control*, J. Lenarčič and M. L. Husty, Eds. Norwell, MA: Kluwer, 1998, pp. 327–336.

[23] F. Tahmasebi and L.-W. Tsai, "Jacobian and stiffness analysis of a novel class of six-DOF parallel minimanipulators," in *Flexible Mechanisms, Dynamics and Analysis*: ASME, 1992, vol. DE-47, pp. 95–102.

[24] N. Simaan, D. Glozman, and M. Shoham, "Design considerations of new six degrees-of-freedom parallel robots," in *Proc. IEEE Int. Conf. Robot. Automat.*, vol. 2, 1998, pp. 1327–1333.

[25] M. Shoham, M. Roffman, S. Goldberger, and N. Simaan, "Robot Structures for Surgery," in *Proc. First Israeli Symp. Computer Assisted Surgery, Medical Robotics and Medical Imaging*, Haifa, Israel, 1998.

[26] N. Simaan and M. Shoham, "Robot construction for surgical applications," in *Proc. Second Israeli Symp. Computer-Aided Surgery, Medical Robotics, and Medical Imaging*, 1999.

[27] N. Simaan, "Analysis and synthesis of parallel robots for medical applications," M.S. thesis, Technion, Haifa, Israel, 1999.

[28] N. Simaan and M. Shoham, "Robot construction for surgical applications," in *Proc. 1st IFAC Conf. Mechatronic Systems*, vol. II, Damstadt, Germany, Sept. 2000, pp. 553–558.

[29] R. I. Alizade, N. R. Tagiyev, and J. Duffy, "A forward and reverse displacement analysis of a 6-DOF in-parallel manipulator," *Mech. Mach. Theory*, vol. 29, no. 1, pp. 115–124, 1994.

[30] O. Veblen and J. W. Young, *Projective Geometry*. Boston, MA: Athenaeum, 1910.

[31] D. M. Y. Sommerville, *Analytical Geometry of Three Dimensions*. Cambridge, U.K.: Cambridge Univ. Press, 1934.

[32] W. C. Graustein, *Introduction to Higher Geometry*. New York: Macmillan, 1930.

[33] H. Pottman, M. Peternell, and B. Ravani, "An introduction to line geometry with applications," *Comput.-Aided Des.*, vol. 31, pp. 3–16, 1999.

[34] J. Phillips, *Freedom In Machinery*. Cambridge, U.K.: Cambridge Univ. Press, 1990.

[35] J.-P. Merlet, "Direct kinematics and assembly modes of parallel manipulators," *Int. J. Robot. Res.*, vol. 11, no. 2, pp. 150–162, 1992.

[36] P. R. McAree and R. W. Daniel, "A fast, robust solution to the Stewart platform forward kinematics," *J. Robot. Syst.*, vol. 11, no. 7, pp. 407–429, 1996.

[37] K. H. Hunt and P. R. McAree, "The octahedral manipulator: geometry and mobility," *Int. J. Robot. Res.*, vol. 17, no. 8, pp. 686–885, 1998.

[38] E. F. Fichter, "A Stewart platform-based manipulator: General theory and practical construction," *Int. J. Robot. Res.*, vol. 5, no. 2, pp. 157–182, 1986.

[39] K. H. Hunt, "Structural kinematics of in-parallel-actuated robot-arms," *ASME J. Mech., Trans. Automat. Des.*, vol. 105, pp. 705–712, 1983.

[40] J. P. Merlet, "Parallel Manipulators, Part 2: Singular Configurations and Grassman Geometry," INRIA Res. , Rep. 791, Feb. 1988.

[41] N. Simaan and M. Shoham, "Analysis and synthesis of parallel robots for medical applications—The RSPR parallel robot," Robot. Lab., Mech. Eng., Technion–Israel Inst. Technol., Haifa, Israel, http://robotics.technion.ac.il.

Nabil Simaan received the B.Sc. and M.Sc. degrees in mechanical engineering from the Technion–Israel Institute of Technology, Haifa, Israel, in 1996 and 1999, respectively. He is currently a Ph.D. candidate at the same institution.

His research interests are focused on the analysis and synthesis problems of parallel robots and general mechanism design. His M.Sc. thesis dealt with synthesis, design, construction, and control of the RSPR robot for medical applications.

Moshe Shoham (M'86) has been conducting research in the robotic field for the past 15 years, with a special focus on kinematics and dynamics, sensor integration, multifinger hands, and medical applications. He has been heading the Robotics Laboratories of the Mechanical Engineering Department at Columbia University, New York, and the Technion-Israel Institute of Technology, Haifa, Israel. His research activity has been funded by grants from several agencies in Israel, the United States, France, and EC.

Dr. Shoham has developed and constructed novel robotic systems for which he received the following awards: the Haifa City Award for Science and Technology, the Mitchell Entrepreneurial Award, the Hershel Rich Innovation Award, and the Jolodan Prize.